Progress In Electromagnetics Research C, Vol. 132, 65–77, 2023

Differential Negative Group Delay Circuit Topology with Reverse Nested Double U-Shaped Defected Ground Structure

Zicheng Wang, Zhongbao Wang*, Hongmei Liu, and Shaojun Fang

Abstract—A simple and flexible differential negative group delay (NGD) circuit topology based on defected ground structure (DGS) is proposed. The circuit consists of microstrip lines and reverse nested double U-shaped (RNDU) DGSs, in which differential transmission and common-mode suppression (CMS) are realized by microstrip lines, and the adjustment of NGD time and center frequency is achieved by changing the RNDU DGSs. Besides, the bandwidth and NGD time can be increased by cascading double couples of RNDU DGSs. For demonstration, two circuit prototypes with single- and double-couple DGSs are fabricated and measured. The measured results show that the NGD time of the single-couple DGS circuit at the center frequency of 2.279 GHz is −0.57 ns; the insertion loss is 2.08 dB; and the NGD bandwidth is 28 MHz. The NGD time of the double-couple DGS circuit at 2.30 GHz is −2.13 ns; the NGD bandwidth is 41 MHz; and the insertion loss is 4.39 dB. The functions of increasing bandwidth and enhancing NGD are realized. The common-mode insertion loss can reach 43.2 dB, and excellent CMS characteristics are achieved.

1. INTRODUCTION

Nowadays, differential circuits are extensively used in various radio frequency (RF) components due to their excellent suppression of common-mode noise from the environment or system [1–4]. In RF systems, different frequency components will cause different phase delays due to the nonlinear group delay (GD) characteristics of the channel, resulting in signal distortion and increased bit error rate [5, 6]. The RF circuit with negative group delay (NGD) characteristics can effectively compensate and improve the GD index of the signal-carrying information transmitted in the circuit. In [7], a crossed resonator interconnect structure was proposed to achieve quad-band NGD characteristics. Based on 180-nm CMOS technology, an inductor-less NGD integrated circuit was designed by using RC-network, metal-insulator-metal capacitor, and polygate resistor [8]. A compact and wideband flat NGD circuit with two resistors that connect the microstrip line and the stepped impedance resonator was proposed in [9], which had a large insertion loss (IL). A power divider of balanced-to-single-ended power dividing network was proposed in [10], which adopted the structure of resistors connecting coupling lines to realize NGD and isolation characteristics. However, it has weak common-mode suppression (CMS). Compared with [10], the CMS has been improved in [11]. However, it has poor isolation and high IL. In [12, 13], multiple coupling lines and transmission lines were used, in which unequal-length transmission lines were used to realize NGD. In [14], a method to realize NGD characteristics based on asymmetric coplanar striplines and double-sided parallel striplines (DSPSs) was proposed. The differential NGD circuit in [15] used coupled lines connecting transmission line stubs with resistors to achieve NGD and CMS. The differential dual-band NGD circuit proposed in [16] used phase shift swap structures, DSPS, and two coupled-line resonators of unequal lengths to achieve the wideband CMS and dual-band NGD.

Received 12 March 2023, Accepted 10 April 2023, Scheduled 13 April 2023
* Corresponding author: Zhongbao Wang (wangzb@dlmu.edu.cn).
The authors are with the School of Information Science and Technology, Dalian Maritime University, Dalian, Liaoning 116026, China.

Recently, defected ground structures (DGSs) have been widely studied to achieve the band gap characteristics and slow wave effect which change the electromagnetic distribution characteristics between the microstrip line and ground plane through the etching cycle or specific pattern on the grounding metal plate [17, 18], and the structure can reduce the circuit size to a certain extent. By changing the size and relative position of the DGS pattern, distribution parameters can be adjusted to achieve NGD characteristics. In [19], a U-shaped defect structure was designed on the ground plane to achieve NGD characteristics, and the NGD time can be adjusted through an external resistor. On this basis, dual-plane defected structures were designed [20] to achieve dual-band NGD characteristics. In [21], NGD circuits based on complementary split ring resonator (CSRR) DGS were designed, and the NGD performances for the DGS formed by single- and double-wing CSRRs were analyzed. Based on the above research, for differential circuits, it is necessary to strengthen the CMS characteristics on the basis of existing research results, increase the return loss while ensuring low insertion loss, improve the comprehensive characteristics of the NGD circuit, and make the circuit design highly flexible, which can be integrated into existing circuits to achieve NGD functions.

In this paper, a differential NGD circuit topology based on DGSs with a reverse nested double U-shaped (RNDU) pattern is proposed. The proposed differential NGD circuit topology consists of single-couple and double-couple RNDU DGSs and microstrip lines. NGD characteristic is achieved through RNDU DGSs and the coupling of RNDU DGSs and microstrip lines. The design method discussed in this paper has certain high flexibility for designing differential circuits that realize NGD characteristics.

2. DESIGN OF THE PROPOSED DIFFERENTIAL NGD CIRCUIT

Figure 1 depicts the proposed differential NGD circuit topology with RNDU DGSs. The circuit is composed of:

1) Microstrip lines (MLs). The top layer uses MLs to realize differential transmission and CMS characteristics. Specifically, there are four microstrip lines as ports, which are connected to the external circuit, two $\lambda_g/2$ microstrip lines, which realize CMS, and two microstrip lines, which ensure the differential transmission and coupled with the DGS to achieve the NGD characteristics.

2) RNDU DGSs. The bottom layer etches RNDU DGSs to couple with MLs at a specific location to realize NGD characteristics. Different NGD indexes can be achieved by changing RNDU DGSs parameters.

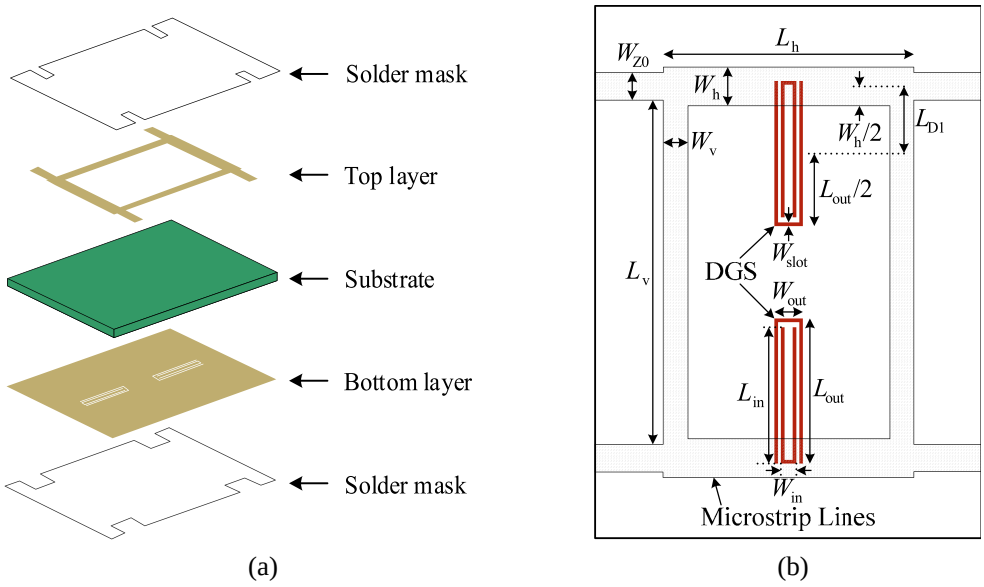

Figure 1. Configuration of the proposed differential NGD circuit. (a) Exploded view. (b) MLs and DGSs.

3) Solder mask. The top and bottom solder mask layers provide a good protective layer for printed circuit board (PCB), so as to avoid short circuited and ensure that the surface of the PCB is not oxidized or damaged.

2.1. Equivalent Circuit Modeling

To analyze the proposed differential NGD circuit, the DGS equivalent circuit model (ECM) proposed in [22] is used, which consists of a parallel inductor L_d, a capacitor C_d, and a resistor R_d connected in series to the circuit, as well as parallel capacitors C_g and resistors R_g connected in parallel to the circuit and ground. As the proposed circuit is a differential circuit, a half-wavelength transmission line with an electrical length of π at the center frequency f_0 is configured at each of the two differential ports to form the differential NGD circuit. Then, the mixed scattering parameter analysis results can be obtained.

Figure 2 shows the differential circuit with the RNDU DGS equivalent circuit. In the equivalent circuit diagram, the DGS is equivalent to the lumped components, and the schematic diagram of the microstrip line is shown. The mixed S-parameters of the proposed differential NGD circuit are

$$\begin{cases} S_{ddAA} = (S_{A+A+} - S_{A+A-} - S_{A-A+} + S_{A-A-})/2 \\ S_{ddBA} = (S_{B+A+} - S_{B+A-} - S_{B-A+} + S_{B-A-})/2 \\ S_{ccAA} = (S_{A+A+} + S_{A+A-} + S_{A-A+} + S_{A-A-})/2 \\ S_{ccBA} = (S_{B+A+} + S_{B+A-} + S_{B-A+} + S_{B-A-})/2 \end{cases} \tag{1}$$

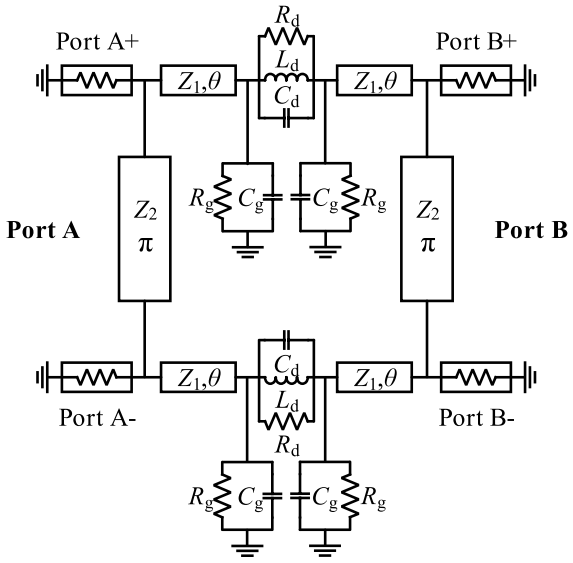

Figure 2. Differential NGD circuit with RNDU DGS equivalent circuits.

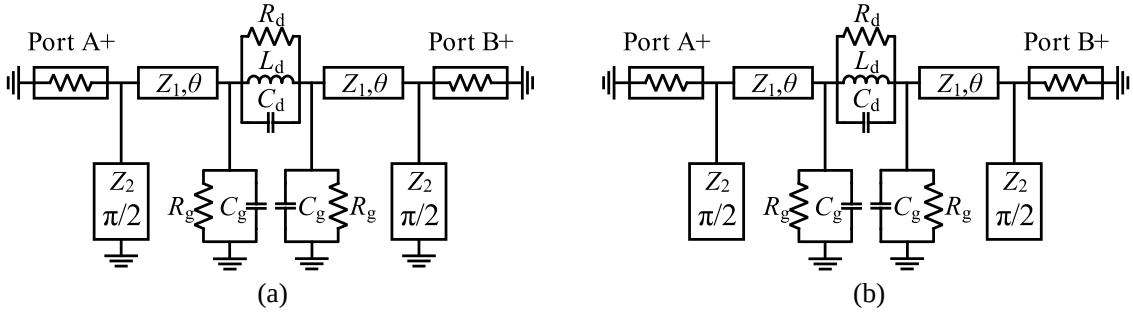

Figure 3. (a) Odd- and (b) even-mode equivalent circuits.

As the circuit is horizontally symmetrical, the circuit can be decomposed as shown in Figure 3 by using the odd- and even-mode method, and the relationship shown in (2) can be obtained.

$$\begin{cases} S_{ddAA} = S_{A+A+\_o} \\ S_{ddBA} = S_{B+A+\_o} \\ S_{ccAA} = S_{A+A+\_e} \\ S_{ccBA} = S_{B+A+\_e} \end{cases} \tag{2}$$

Defining Y_l as the admittance of the microstrip line with characteristic impedance Z_2, Y_g as the parallel admittance of C_g and R_g, and Z_d as the parallel impedance of R_d, L_d and C_d, the transfer parameter matrix of the proposed differential NGD equivalent circuit is expressed as

$$\begin{bmatrix} A_T & B_T \\ C_T & D_T \end{bmatrix} = \begin{bmatrix} 1 & 0 \\ Y_l & 1 \end{bmatrix} \begin{bmatrix} A & B \\ C & A \end{bmatrix} \begin{bmatrix} 1 & 0 \\ Y_g & 1 \end{bmatrix} \begin{bmatrix} 1 & Z_d \\ 0 & 1 \end{bmatrix} \begin{bmatrix} 1 & 0 \\ Y_g & 1 \end{bmatrix} \begin{bmatrix} A & B \\ C & A \end{bmatrix} \begin{bmatrix} 1 & 0 \\ Y_l & 1 \end{bmatrix}$$

$$= \begin{bmatrix} A^2 + 2ABY_g + A^2Z_dY_g + ABY_g^2Z_d + ACZ_d + \\ BCY_gZ_d + BC + 2ABY_l + 2B^2Y_gY_l + A^2Z_dY_l + \\ B^2Y_g^2Z_dY_l + 2ABZ_dY_gY_l & 2AB + 2B^2Y_g + A^2Z_d + 2ABZ_dY_g + \\ & B^2Y_g^2Z_d \\ 2A^2Y_l + 2A^2Y_g + 4ABY_gY_l + 2ACZ_dY_g + \\ A^2Y_g^2Z_d + 2A^2Y_gY_lZ_d + 2ABY_lY_g^2Z_d + \\ 2AC + 2ACY_lZ_d + C^2Z_d + 2BCY_lY_gZ_d + \\ 2BCY_l + 2ABY_l^2 + 2B^2Y_l^2Y_g + A^2Y_l^2Z_d + \\ B^2Y_l^2Y_g^2Z_d + 2ABY_l^2Y_gZ_d & A^2 + 2ABY_g + A^2Z_dY_g + ABY_g^2Z_d + \\ & ACZ_d + BCY_gZ_d + BC + 2ABY_l + \\ & 2B^2Y_gY_l + A^2Z_dY_l + B^2Y_g^2Z_dY_l + \\ & 2ABZ_dY_gY_l \end{bmatrix} \tag{3}$$

where

$$Y_l = \begin{cases} \frac{1}{\mathrm{j}Z_2 \tan\left(\frac{\pi}{2}\frac{f}{f_0}\right)} & \text{For odd mode} \\ \frac{1}{-\mathrm{j}Z_2 \cot\left(\frac{\pi}{2}\frac{f}{f_0}\right)} & \text{For even mode} \end{cases} \tag{4}$$

$$A = \cos\theta, \;\; B = \mathrm{j}Z_1 \sin\theta, \;\; C = \mathrm{j}\frac{1}{Z_1}\sin\theta \tag{5}$$

$$Y_g = \frac{1 + \mathrm{j}\omega C_g R_g}{R_g}, \;\; Z_d = \frac{\mathrm{j}\omega L_d R_d}{R_d + \mathrm{j}\omega L_d - \omega^2 L_d C_d R_d} \tag{6}$$

Using parameter conversion to obtain scattering parameters

$$S_{A+A+\_o} = \frac{\begin{array}{c} \frac{2AB}{Z_0} + \frac{2B^2Y_g}{Z_0} + \frac{A^2Z_d}{Z_0} + \frac{2ABZ_dY_g}{Z_0} + \frac{B^2Y_g^2Z_d}{Z_0} - 2A^2Y_lZ_0 - 2A^2Y_gZ_0 - 4ABY_gY_lZ_0 - \\ 2ACZ_dY_gZ_0 - 2A^2Y_gY_lZ_dZ_0 - A^2Y_g^2Z_dZ_0 - 2ABY_lY_g^2Z_dZ_0 - 2ACZ_0 - 2ACY_lZ_dZ_0 - \\ C^2Z_dZ_0 - 2BCY_lY_gZ_dZ_0 - 2BCY_lZ_0 - 2ABY_l^2Z_0 - 2B^2Y_l^2Y_gZ_0 - 2ABY_l^2Y_gZ_dZ_0 - \\ B^2Y_l^2Y_g^2Z_dZ_0 - A^2Y_l^2Z_dZ_0 \end{array}}{\begin{array}{c} 2A^2 + 4ABY_g + 2A^2Z_dY_g + 2ABY_g^2Z_d + 2ACZ_d + 2BCY_gZ_d + 2BC + 4ABY_l + 4B^2Y_gY_l + \\ 2A^2Z_dY_l + 2B^2Y_g^2Z_dY_l + 4ABZ_dY_gY_l + \frac{2AB}{Z_0} + \frac{2B^2Y_g}{Z_0} + \frac{A^2Z_d}{Z_0} + \frac{2ABZ_dY_g}{Z_0} + \frac{B^2Y_g^2Z_d}{Z_0} + \\ 2A^2Y_lZ_0 + 2A^2Y_gZ_0 + 4ABY_gY_lZ_0 + 2ACZ_dY_gZ_0 + A^2Y_g^2Z_dZ_0 + 2A^2Y_gY_lZ_dZ_0 + 2ACZ_0 + \\ 2ABY_lY_g^2Z_dZ_0 + 2ACY_lZ_dZ_0 + C^2Z_dZ_0 + 2BCY_lY_gZ_dZ_0 + 2BCY_lZ_0 + 2ABY_l^2Z_0 + \\ 2B^2Y_l^2Y_gZ_0 + A^2Y_l^2Z_dZ_0 + B^2Y_l^2Y_g^2Z_dZ_0 + 2ABY_l^2Y_gZ_dZ_0 \end{array}} \tag{7}$$

$$S_{B+A+\_o} = \frac{2}{\begin{array}{c}2A^2+4ABY_g+2A^2Z_dY_g+2ABY_g^2Z_d+2ACZ_d+2BCY_gZ_d+2BC+4ABY_l+4B^2Y_gY_l+\\ 2A^2Z_dY_l+2B^2Y_g^2Z_dY_l+4ABZ_dY_gY_l+\frac{2AB}{Z_0}+\frac{2B^2Y_g}{Z_0}+\frac{A^2Z_d}{Z_0}+\frac{2ABZ_dY_g}{Z_0}+\frac{B^2Y_g^2Z_d}{Z_0}+\\ 2A^2Y_lZ_0+2A^2Y_gZ_0+4ABY_gY_lZ_0+2ACZ_dY_gZ_0+A^2Y_g^2Z_dZ_0+2A^2Y_gY_lZ_dZ_0+2ACZ_0+\\ 2ABY_lY_g^2Z_dZ_0+2ACY_lZ_dZ_0+C^2Z_dZ_0+2BCY_lY_gZ_dZ_0+2BCY_lZ_0+2ABY_l^2Z_0+\\ 2B^2Y_l^2Y_gZ_0+A^2Y_l^2Z_dZ_0+B^2Y_l^2Y_g^2Z_dZ_0+2ABY_l^2Y_gZ_dZ_0\end{array}} \tag{8}$$

From Equations (2), (3), (4), (7), and (8),

$$S_{ddAA} = \frac{\begin{array}{c}\frac{2AB}{Z_0}+\frac{2B^2Y_g}{Z_0}+\frac{A^2Z_d}{Z_0}+\frac{2ABZ_dY_g}{Z_0}+\frac{B^2Y_g^2Z_d}{Z_0}{}_0-2A^2Y_gZ_0-2ACZ_dY_gZ_0-\\ A^2Y_g^2Z_dZ_0-2ACZ_0-C^2Z_dZ_0\end{array}}{\begin{array}{c}2A^2+4ABY_g+2A^2Z_dY_g+2ABY_g^2Z_d+2ACZ_d+2BCY_gZ_d+2BC+\frac{2AB}{Z_0}+\\ \frac{2B^2Y_g}{Z_0}+\frac{A^2Z_d}{Z_0}+\frac{2ABZ_dY_g}{Z_0}+\frac{B^2Y_g^2Z_d}{Z_0}+2A^2Y_gZ_0+2ACZ_dY_gZ_0+A^2Y_g^2Z_dZ_0+\\ 2ACZ_0+C^2Z_dZ_0\end{array}} \tag{9}$$

$$S_{ddBA} = \frac{2}{\begin{array}{c}2A^2+4ABY_g+2A^2Z_dY_g+2ABY_g^2Z_d+2ACZ_d+2BCY_gZ_d+2BC+\frac{2AB}{Z_0}+\\ \frac{2B^2Y_g}{Z_0}+\frac{A^2Z_d}{Z_0}+\frac{2ABZ_dY_g}{Z_0}+\frac{B^2Y_g^2Z_d}{Z_0}+2A^2Y_gZ_0+2ACZ_dY_gZ_0+A^2Y_g^2Z_dZ_0+\\ 2ACZ_0+C^2Z_dZ_0\end{array}} \tag{10}$$

$$S_{ccAA} \approx -1 \tag{11}$$

$$S_{ccBA} \approx 0 \tag{12}$$

According to Equations (9)–(12), this circuit can realize differential-mode transmission and common-mode suppression characteristics.

The differential group delay is expressed as

$$\tau = -\frac{1}{2\pi}\frac{\mathrm{d}\angle S_{ddBA}(f)}{\mathrm{d}f} \tag{13}$$

According to the conditional formula of the resonant circuit

$$f_0 = \frac{1}{2\pi\sqrt{L_dC_d}} \tag{14}$$

The NGD performance of the equivalent circuit is mainly determined by L_d, C_d, and R_d. The NGD center frequency is determined by adjusting L_d and C_d, and the depth of NGD is determined by the value of R_d. Besides, C_g and R_g are minuscule equivalent capacitances and non-negligible equivalent resistances, respectively. Assume that the NGD characteristic is realized at the 2.29 GHz center frequency and that NGD time is −0.55 ns. By optimizing parameters through MATLAB and ADS software according to the expression and circuit, the results of L_d, C_d, C_g, R_g, and R_d are 28.24 pH, 171 pF, 0.0061 pF, 0.10 MΩ, and 17.46 Ω, respectively.

2.2. Circuit Design and Parametric Analysis

The purpose of adopting RNDU DGSs is to achieve NGD characteristics. As shown in Figure 1(b), the outer and inner structures' lengths and widths of the RNDU pattern are L_{out}, W_{out}, L_{in}, and W_{in}, respectively. The slot width of outer and inner RNDU DGSs is W_{slot}. According to the equivalent circuit shown in Figure 2, this structure can be equivalent to a parallel RLC resonant network in series in the circuit to generate NGD characteristics. Therefore, the center frequency and GD are determined by the equivalent resistance, capacitance, and inductance. With changing the sizes of the RNDU DGSs, equivalent resistance, capacitance, and inductance of the DGS are changed; meanwhile, the center

frequency and GD are changed. In this design, the effective length of a single DGS is defined as L_{DGS}, and the formula defined by L_{DGS} is

$$L_{\mathrm{DGS}} = L_{\mathrm{out}} \times 2 + L_{\mathrm{in}} + W_{\mathrm{in}} \tag{15}$$

The solder mask is used in the prototype circuit, whose relative dielectric constant is 4.85, loss tangent 0.023, and thickness 15 μm. As shown in Figure 4, the use of a solder mask will affect the NGD center frequency of the differential NGD circuit.

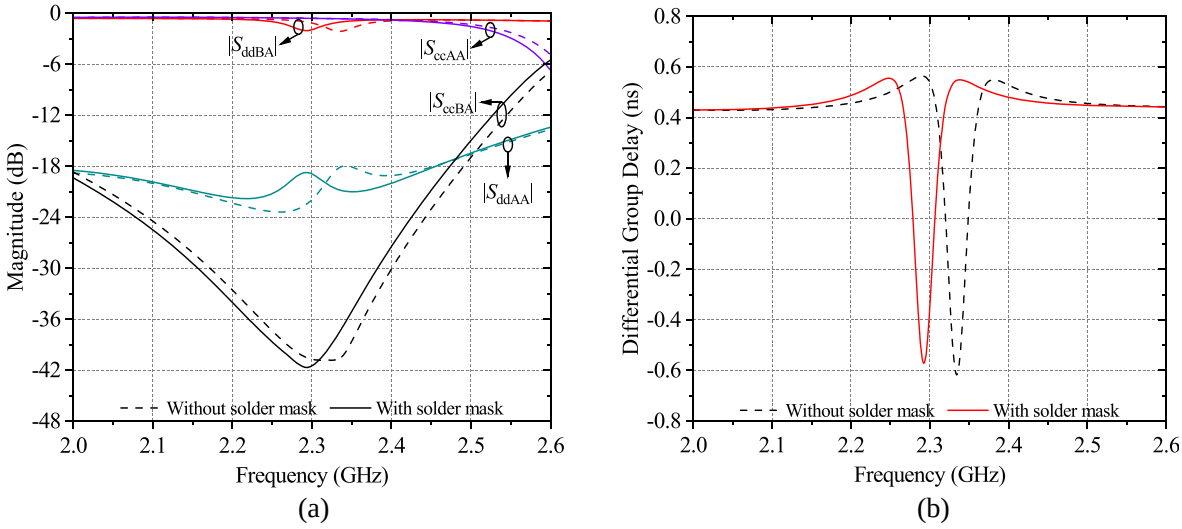

Figure 4. Effect of solder mask on the performance of the proposed circuit. (a) Mixed S-parameters. (b) GD.

For the RNDU DGS pattern, changing the size of the RNDU DGS determines the NGD center frequency. Adjusting the L_{DGS} and obtaining the relationship between L_{DGS} and the NGD center frequency through simulation is shown in Figure 5. In order to demonstrate the influence of changing L_{DGS} on the NGD center frequency, change L_{out} and L_{in} while keeping W_{out}, W_{in}, and W_{slot} invariant, and change L_{D1} at the same time to ensure that the projected area of DGS below the microstrip line remains invariant.

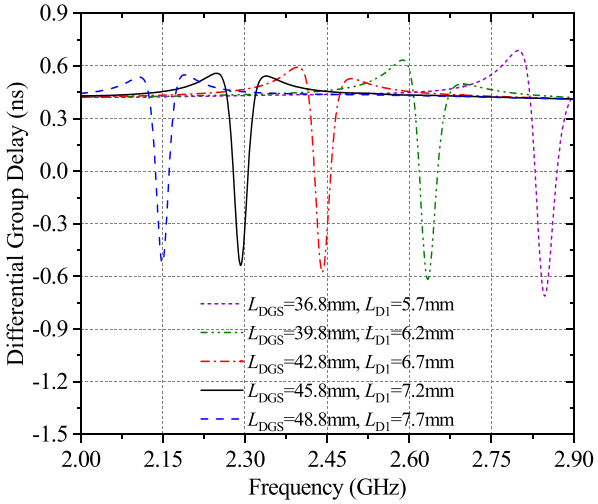

Figure 5. Effect of L_{DGS} on the NGD center frequency of the proposed circuit.

According to the simulation results, in this design, the NGD center frequency depends on the size of each part of the DGS structure, and the sorting estimation formula is

$$L_{\mathrm{DGS}} = L_{\mathrm{out}} \times 2 + L_{\mathrm{in}} + W_{\mathrm{in}} \approx \frac{\lambda_g}{2} \tag{16}$$

In Equation (16), L_{DGS} is approximately equal to half of λ_g, which corresponds to the NGD center frequency f_0 in Equation (14). Therefore, in the process of equivalent circuit simulation to DGS pattern design, the NGD center frequency can be determined in the equivalent circuit based on L_d and C_d, and the relational expression corresponds to L_{out}, L_{in}, and W_{in} of the DGS geometrical parameters. After determining the center frequency of NGD, the NGD time is controlled by the distance L_{D1} between the center of RNDU DGS and the microstrip lines. The relationship between L_{D1} and NGD time of the differential circuit with single-couple DGS is analyzed and shown in Figure 6.

The W_h and L_h of the top layer microstrip lines shown in Figure 1(b) affect the coupling with the bottom layer DGS structure. Figures 7 and 8 show the influence of L_h and W_h on mixed S-parameter and GD when the DGS structure position and dimensions are invariant. It can be found that changing

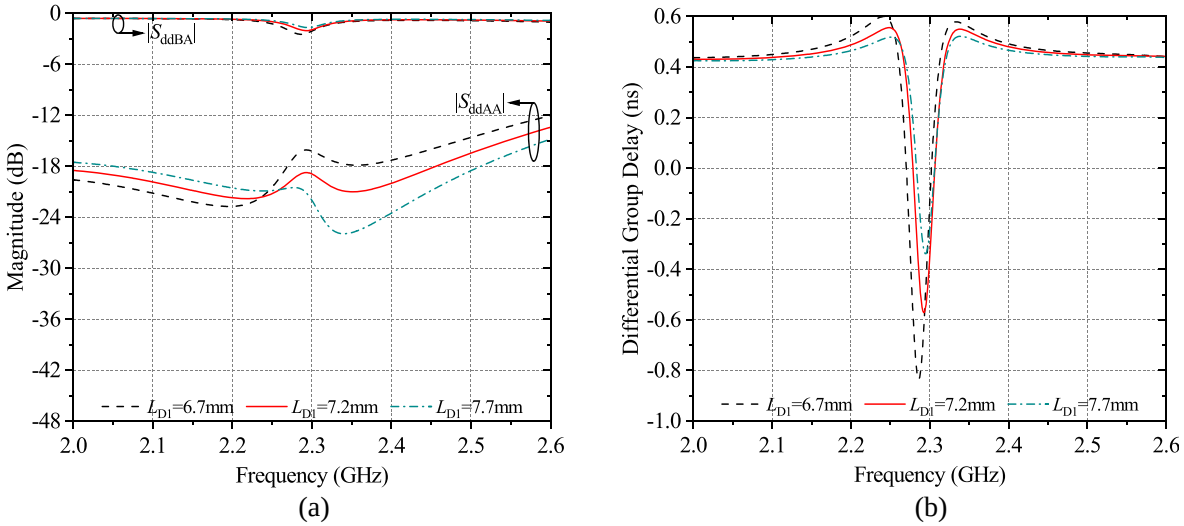

Figure 6. Effect of L_{D1} on the performance of the proposed circuit. (a) Mixed S-parameters, (b) GD.

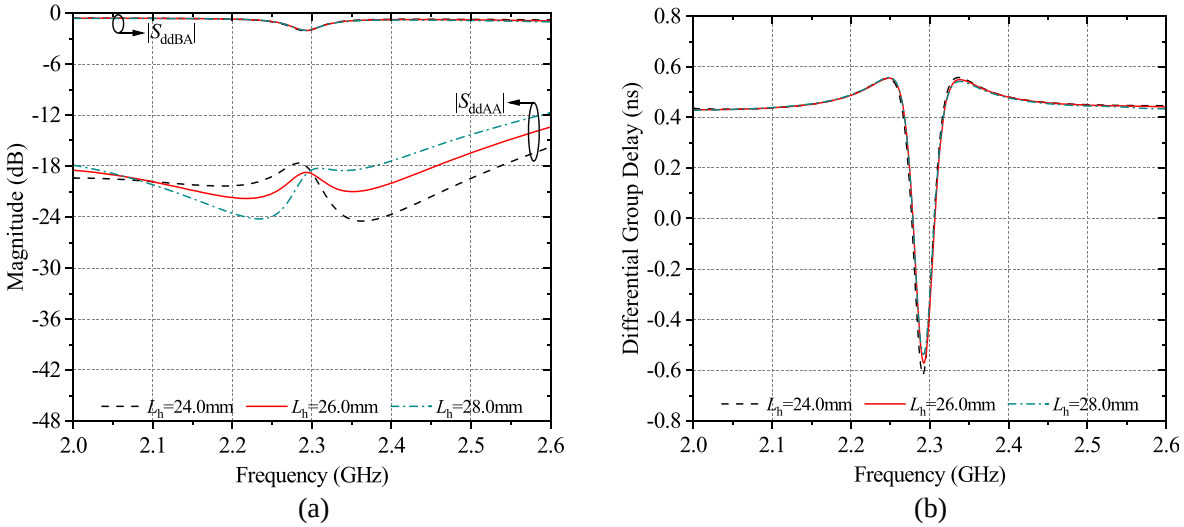

Figure 7. Effect of L_h on the performance of the proposed circuit. (a) Mixed S-parameters, (b) GD.

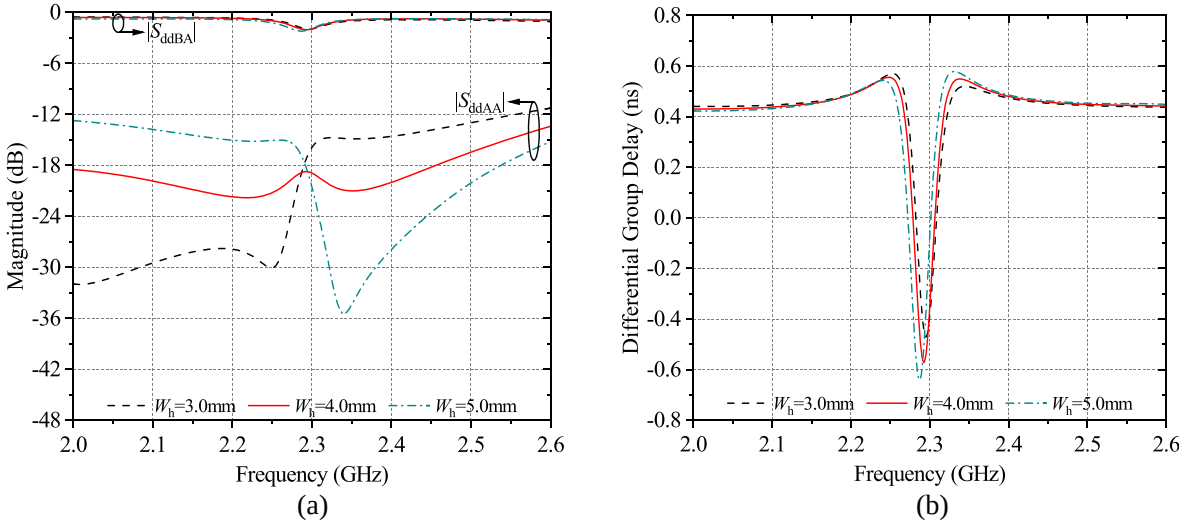

Figure 8. Effect of W_h on the performance of the proposed circuit. (a) Mixed S-parameters, (b) GD.

W_h and L_h has a slight impact on the insertion loss, but has a great influence on the $|S_{ddAA}|$. In the application, appropriate W_h and L_h should be selected for a preferable return loss.

2.3. Circuit Design Procedure

The differential circuit design method with the RNDU DGSs which realize the NGD characteristics discussed in this paper is summarized in the following 5 steps:

1) Confirm the NGD center frequency, required NGD value, and acceptable mixed S-parameters characteristics.

2) Select the substrate material of the PCB (FR-4 is recommended), and calculate the microstrip line width of the 4-ports according to the characteristic impedance of the ports.

3) Design the length and width of the microstrip line of the proposed circuit on the top layer and the DGS dimensions and relative position on the bottom layer according to the specified NGD center frequency, required NGD value, and Figures 5–8.

4) Use electromagnetic simulation software, such as ANSYS HFSS, to simulate the circuit and optimize the circuit parameters according to the circuit/system requirements.

5) Manufacture and test the circuit optimized by the simulation in the previous step to realize the final demand.

3. SIMULATION AND EXPERIMENTAL RESULTS

To validate the proposed concept, two differential NGD circuit prototypes based on RNDU DGSs are designed, simulated, manufactured, and measured. The circuits are described in detail in the following two subsections.

3.1. Differential NGD Circuit with Single-Couple DGS

The designing for a single-couple DGS differential NGD circuit with a size of $40 \times 55 \times 1.6\,\text{mm}^3$ used an FR-4 epoxy substrate with a relative dielectric constant of 4.8 and loss tangent of 0.025. The used solder mask has a relative dielectric constant of 4.85, a loss tangent of 0.023, and a thickness of 15 μm.

According to the circuit design procedure, determine the length and width of the microstrip line on the top layer and the specific size of the RNDU DGS pattern of the bottom layer by using ANSYS HFSS electromagnetic (EM) simulation software, and the prototype circuit dimensions shown in Table 1 are obtained after the calculation, simulation, and optimization of parameters. The manufactured differential NGD circuit with single-couple RNDU DGS is shown in Figure 9. The prototype circuit

Table 1. Dimensions of the proposed differential NGD circuit with single-couple RNDU DGS. (Unit: mm).

W_{Z0}	L_h	W_h	L_v	W_v	L_{out}	L_{in}	W_{out}	W_{in}	W_{slot}	L_{D1}
2.86	26.00	4.00	35.64	2.50	15.10	14.10	3.00	1.50	0.40	7.20

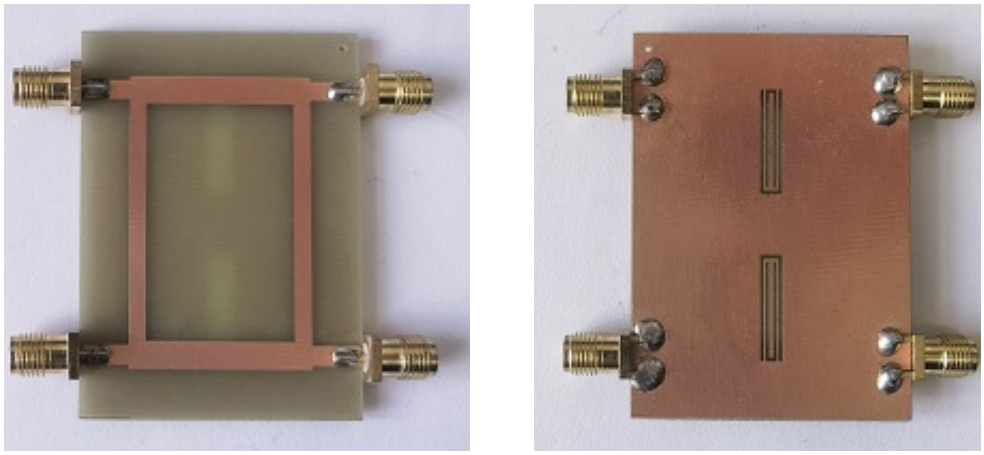

Figure 9. Prototype photograph of the proposed differential NGD circuit with single-couple RNDU DGS. (a) Top layer. (b) Bottom layer.

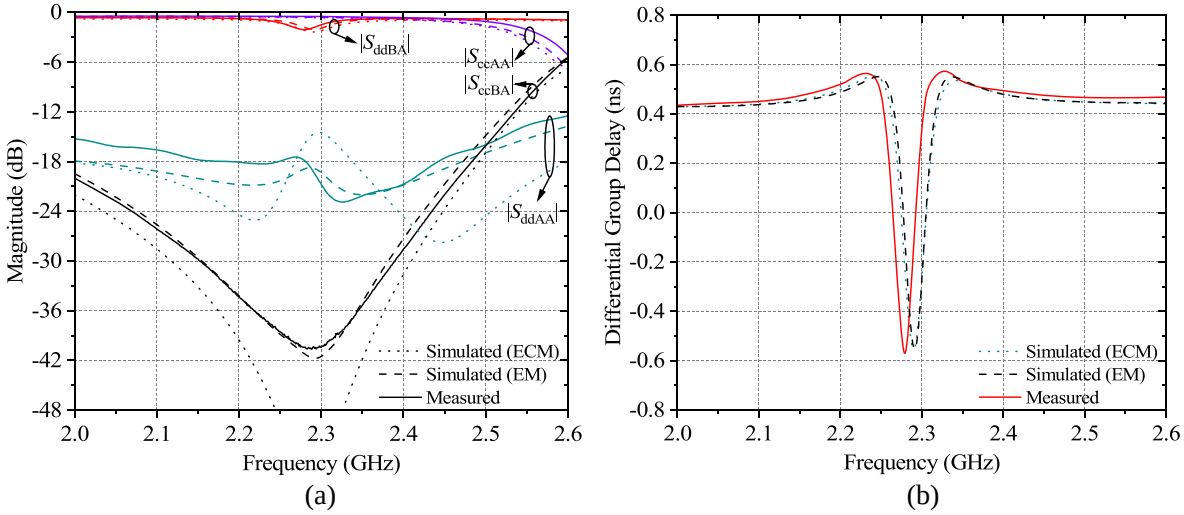

Figure 10. Simulated and measured results of the proposed differential NGD circuit with single-couple RNDU DGS. (a) Mixed S-parameters. (b) GD.

is measured by Agilent Technologies N5230A PNA-L vector network analyzer. Figure 10 shows the simulation and measurement results of mixed S-parameters and GD of the proposed differential NGD circuit with single-couple RNDU DGS. At the NGD center frequency $f_0 = 2.279$ GHz, the measured differential GD is -0.57 ns; the measured differential-mode insertion loss is 2.08 dB; the measured differential-mode return loss is 17.8 dB; the measured common-mode return loss is 0.52 dB; and the measured common-mode insertion loss (i.e., CMS) is 40.4 dB. The bandwidth for differential group delay less than 0 ns is 28 MHz from 2.265 to 2.293 GHz.

3.2. Differential NGD Circuit with Double-Couple RNDU DGS

To improve the bandwidth and group delay performance on the basis of single-couple DGS differential NGD circuit topology, increasing the number of RNDU DGS can be adopted. Because one couple of DGS can realize NGD characteristics on a central frequency, the NGD central frequency is controlled by L_{DGS}. If the L_{DGS} values of different couples of DGS are close, the NGD center frequencies controlled by different couples are close. Thus, NGD and bandwidth characteristics are the superposition of NGD and bandwidth controlled by different couples respectively. In order to verify this scheme, a differential NGD circuit with double-couple RNDU DGS as shown in Figures 11 and 12 is designed and manufactured to increase the bandwidth and enhance the NGD characteristics. The circuit dimensions are shown in Table 2. The overall circuit size is $40 \times 55 \times 1.6\,\mathrm{mm}^3$.

Figure 13 shows the simulation and measurement results of mixed S-parameters and GD of the proposed differential NGD circuit with double-couple RNDU DGS. At the NGD center frequency

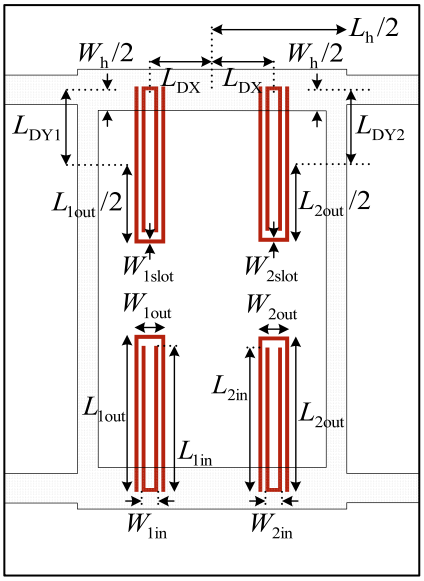

Figure 11. Structure of the proposed differential NGD circuit with double-couple RNDU DGS.

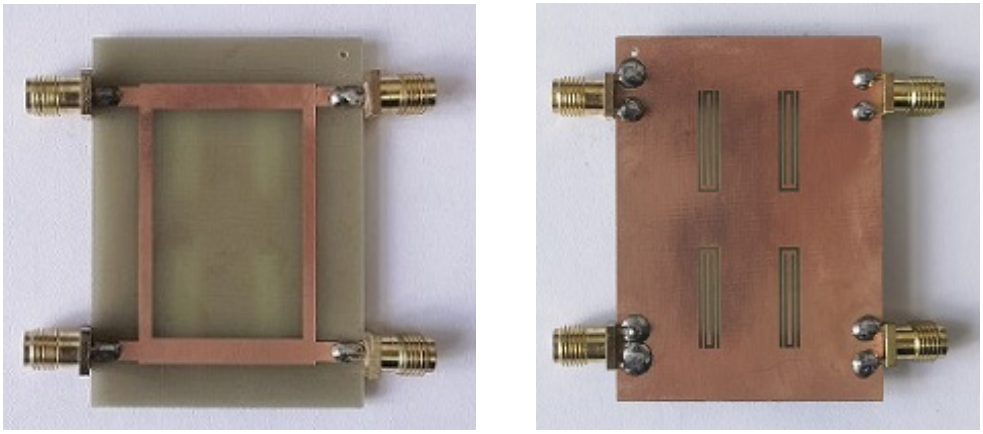

(a) (b)

Figure 12. Photograph of the proposed differential NGD circuit with double-couple RNDU DGS. (a) Top layer. (b) Bottom layer.

Table 2. Dimensions of the proposed differential NGD circuit with double-couple RNDU DGS. (Unit: mm).

W_{Z0}	L_h	W_h	L_v	W_v	L_{1out}	L_{1in}	W_{1out}	W_{1in}
2.86	26.00	4.00	35.64	2.00	15.10	14.10	3.00	1.50
W_{1slot}	L_{2out}	L_{2in}	W_{2out}	W_{2in}	W_{2slot}	L_{DX}	L_{DY1}	L_{DY2}
0.40	14.97	13.97	3.00	1.50	0.40	6.00	7.20	7.20

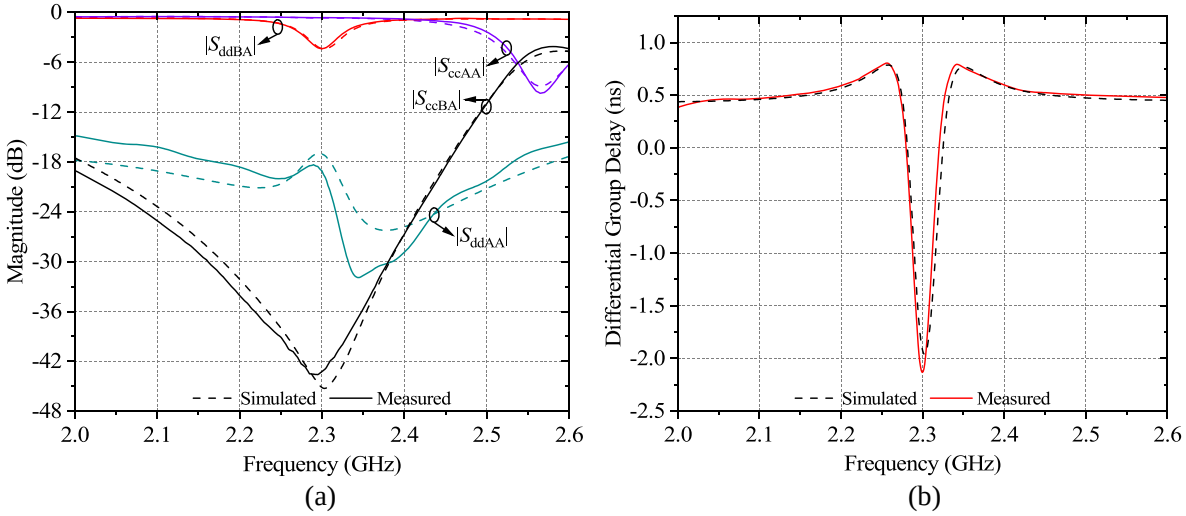

Figure 13. Simulated and measured results of the proposed differential NGD circuit with double-couple RNDU DGS. (a) Mixed S-parameters, (b) GD.

Table 3. Comparison of the proposed differential NGD circuit with previous works.

Reference	f_0 (GHz)	RL (dB)	IL (dB)	NGD (ns)	CMS (dB)	NGD-FBW/ 3 dB FBW (%)	FOM	Size ($\lambda_g \times \lambda_g$)	Differential circuit	Flexible design	Use of resistor
[9]	0.680	14.1	15.3	−0.49	-	42.6/37.4	0.0268	0.20 × 0.38	No	-	Yes
[10]	1.800	15.0	2.40	−1.1	15	1.9/-	0.021	0.25 × 0.55	Yes	-	Yes
[11]	1.000	25.7	7.8	−2.06	37.3	4.0/9.35	0.034	0.57 × 0.30	Yes	-	Yes
[12]	2.436	12.6	2.13	−4.1	-	0.49/-	0.0381	1.47 × 1.26	No	-	No
	3.022	12.4	2.86	−3.8		0.43/-	0.0358				
[13]	1.970	14.0	2.20	−1.0	-	1.02/-	0.0155	0.31 × 1.25	No	Yes	No
[14]	1.579	11.7	4.75	−2.4	-	2.28/7.77	0.0504	0.38 × 0.25	No	Yes	No
[15]	1.000	10.5	3.70	−0.22	18	8.8/-	0.0126	-	Yes	No	Yes
[16]	1.227	14.5	2.49	−1.60	30.8	1.47/-	0.0217	0.41 × 0.30	Yes	Yes	No
	1.575	13.3	3.55	−1.43		1.46/-	0.0222				
[20]	3.500	-	47.2	−4.5	-	3.43/2.93	0.0023	0.64 × 0.36	No	Yes	Yes
	5.150	-	38.8	−4.2	-	1.94/1.43	0.0048				
[21]	2.460	14.0	2.68	−1.9	-	1.42/-	0.0488	0.47 × 0.22	No	Yes	No
This work	**2.300**	**19.1**	**4.39**	**−2.13**	**43.2**	**1.78/4.43**	**0.0527**	**0.58 × 0.80**	**Yes**	**Yes**	**No**

$f_0 = 2.30$ GHz, the measured differential GD is -2.13 ns; the measured differential-mode insertion loss is 4.39 dB; the measured differential-mode return loss is 19.1 dB; the measured common-mode return loss is 0.63 dB; and the measured CMS is 43.24 dB. The differential NGD bandwidth is 41 MHz from 2.280 to 2.321 GHz. It can be seen from the comparison of simulated and measured results that there is a certain deviation between the two results, which is caused by the deviation of the electrical performance parameters of the FR-4 substrate and the discontinuity of the SMA connector solder joints.

The figure of merit (FOM) is usually used to evaluate the comprehensive index and performance of NGD circuits. The FOM of unbalanced and balanced circuits is respectively defined as

$$\text{FOM} = |\text{NGD}(f_0)| \times \text{BW}_{\text{NGD}} \times |S_{21}(f_0)| \tag{17}$$

$$\text{FOM} = |\text{NGD}(f_0)| \times \text{BW}_{\text{NGD}} \times |S_{ddBA}(f_0)| \tag{18}$$

In addition, when a time-domain pulse (e.g., amplitude-modulated Gaussian pulse) passes through an NGD circuit with IL variation much more than 3 dB in the NGD bandwidth, an unacceptable distortion may occur [23]. Therefore, the 3-dB bandwidth should also be used to compare the NGD circuits.

Table 3 shows the comparison between this work and the previous designs. The comparison shows that the proposed differential NGD circuit with RNDU DGS has high return loss while maintaining relatively low insertion loss, good CMS characteristics, excellent FOM evaluation index, and flexible design features.

4. CONCLUSION

In this paper, differential NGD circuits with RNDU DGSs have been presented. The proposed differential NGD circuit has a simple structure and flexible design, which only consists of MLs and RNDU DGS without resistors. The differential transmission and CMS performances are achieved by MLs, and NGD characteristic is produced and dominated by RNDU DGSs' dimensions and relative coordinate with MLs. Two differential NGD circuits with RNDU DGSs have been designed, manufactured, and measured. The measurement results show that the proposed differential NGD circuit has large FOM, good CMS, and high return loss. Therefore, it can be applied in differential circuits and systems to improve group delay characteristics and system performance.

ACKNOWLEDGMENT

This work was supported by the National Natural Science Foundation of China (No. 61871417), the LiaoNing Revitalization Talents Program (No. XLYC2007024), the Natural Science Foundation of Liaoning Province (No. 2020-MS-127), and the Fundamental Research Funds for the Central Universities (No. 3132022243).

REFERENCES

1. Shi, J. and Q. Xue, "Balanced bandpass filters using center-loaded half wavelength resonators," *IEEE Trans. Microwave Theory Tech.*, Vol. 58, No. 4, 970–977, Apr. 2010.
2. Feng, W., W. Che, and Q. Xue, "New balance-applications for dual-mode ring resonators in planar balanced circuits," *IEEE Microw. Mag.*, Vol. 20, No. 7, 15–23, Jul. 2019.
3. Li, L., L.-S. Wu, J. Mao, M. Tang, and X.-W. Gu, "A balanced-to-balanced rat-race coupling network based on defected slots," *IEEE Microwave Wireless Compon. Lett.*, Vol. 29, No. 7, 459–461, Jul. 2019.
4. Shi, J., J. Ren, J. Dong, W. Feng, and Y. Yang, "Supercompact balanced wideband bandpass filter using capacitor-loaded three-line coupled structure," *IEEE Microwave Wireless Compon. Lett.*, Vol. 32, No. 6, 499–502, Jun. 2022.
5. Azizzadeh, A. and L. Mohammadi, "Degradation of BER by group delay in digital phase modulation," *Fourth Advanced International Conference on Telecommunications*, 350–354, Jun. 2008.

6. Myoung, S.-S., Y.-H. Kim, and J.-G. Yook, "Impact of group delay in RF BPF on impulse radio systems," *IEEE MTT-S International Microwave Symposium*, 1891–1894, Jun. 2005.
7. Gu, T., J. Chen, B. Ravelo, F. Wan, V. Mordachev, and Q. Ji, "Quad-band NGD investigation on crossed resonator interconnect structure," *IEEE Trans. Circuits Syst. II, Exp. Briefs*, Vol. 69, No. 12, 4789–4793, Dec. 2022.
8. Wan, F., et al., "Design and experimentation of inductorless low-pass NGD integrated circuit in 180-nm CMOS technology," *IEEE Trans. Comput. Aided Des. Integr. Circuits Syst.*, Vol. 41, No. 11, 4965–4974, Nov. 2022.
9. Gu, T., F. Wan, J. Chen, B. Ravelo, and X. Zhao, "Compact and wideband flat negative group delay circuit investigation," *IEEE Trans. Circuits Syst. II, Exp. Briefs*, Early Access, 2023.
10. Chen, Z., J. Shi, and K. Xu, "Negative group delay power dividing network with balanced-to-single-ended topology," *IET Microw. Antennas Propag.*, Vol. 13, No. 10, 1705–1710, Aug. 2019.
11. Zhu, Z., Z. Wang, S. Zhao, H. Liu, and S. Fang, "A novel balanced-to-unbalanced negative group delay power divider with good common-mode suppression," *Int. J. RF Microw. Comput. Aided Eng.*, Vol. 32, No. 7, e23173, Jul. 2022.
12. Zhou, X., B. Li, N. Li, et al., "Analytical design of dual-band negative group delay circuit with multi-coupled lines," *IEEE Access*, Vol. 8, 72749–72756, 2020.
13. Wan, F., N. Li, B. Ravelo, N. M. Murad, and W. Rahajandraibe, "NGD analysis of turtle-shape microstrip circuit," *IEEE Trans. Circuits Syst. II, Exp. Briefs*, Vol. 67, No. 11, 2477–2481, Nov. 2020.
14. Wang, Z., Y. Bai, Y. Meng, S.-J. Fang, and H. Liu, "A compact negative group delay circuit topology based on asymmetric coplanar striplines and double-sided parallel striplines," *Progress In Electromagnetics Research Letters*, Vol. 98, 139–144, 2021.
15. Zhu, Z., Z. Wang, Y. Meng, S. Fang, and H. Liu, "Balanced microstrip circuit with differential negative group delay characteristics," *Cross Strait Radio Science and Wireless Technology Conference*, 257–259, Oct. 2021.
16. Wang, Z., S. Zhao, H. Liu, and S. Fang, "A compact dual-band differential negative group delay circuit with wideband common mode suppression," *IEEE J. Microw.*, Vol. 2, No. 4, 720–725, Oct. 2022.
17. Li, L., J. Mao, M. Tang, and H. Dai, "Mixed-mode property of defected ground structure and its application in balanced network design with harmonic suppression," *IEEE Microwave Wireless Compon. Lett.*, Vol. 28, No. 3, 188–190, Mar. 2018.
18. Mouris, B. A., A. Fernández-Prieto, R. Thobaben, J. Martel, F. Mesa, and O. Quevedo-Teruel, "Glide symmetry to improve the bandgap operation of periodic microstrip defected ground structures," *European Microwave Conference*, 483–486, Jan. 2021.
19. Chaudhary, G., J. Jeong, P. Kim, Y. Jeong, and J. Lim, "Compact negative group delay circuit using defected ground structure," *Asia-Pacific Microwave Conference*, 22–24, Nov. 2013.
20. Chaudhary, G., Y. Jeong, and J. Lim, "Miniaturized dual-band negative group delay circuit using dual-plane defected structures," *IEEE Microwave Wireless Compon. Lett.*, Vol. 24, No. 8, 521–523, Aug. 2014.
21. Ji, Q., et al., "CSRR DGS-based bandpass negative group delay circuit design," *IEEE Access*, Vol. 11, 20309–20318, 2023.
22. Park, J., J. Kim, J. Lee, S. Kim, and S. Myung, "A novel equivalent circuit and modeling method for defected ground structure and its application to optimization of a DGS lowpass filter," *IEEE MTT-S International Microwave Symposium*, 417–420, Jun. 2002.
23. Kandic, M. and G. E. Bridges, "Negative group delay prototype filter based on cascaded second order stages implemented with Sallen-Key topology," *Progress In Electromagnetics Research B*, Vol. 94, 1–18, 2021.